Research Article

Jinshan Che*, Mingming Sun, and Zhipan Li

Development of a point-of-care testing sensor using polypyrrole/TiO_2 molecular imprinting technology for cinchocaine determination

https://doi.org/10.1515/revac-2025-0087
received February 22, 2025; accepted July 16, 2025

Abstract: An electrochemical sensor for cinchocaine (CIN) detection was developed based on surface molecular imprinting technology utilizing screen-printed gold electrodes modified with TiO_2 nanoparticles and electropolymerized polypyrrole. A novel sensor was developed using a dual-stage methodology, which entailed initial CIN template immobilization and subsequent electrochemical pyrrole polymerization incorporating titanium dioxide nanoscale particles. The sensor exhibited enhanced electroactive surface area (0.075 cm^2) and improved electron transfer kinetics (heterogeneous rate constant 8.2×10^{-3} $cm \cdot s^{-1}$) compared to unmodified electrodes. Under optimized conditions (pH 5.0, 15-min incubation), the sensor demonstrated two linear response ranges from 0.1–10 and 10–100 μM, with a detection limit of 0.035 μM. The sensor showed excellent selectivity against common interferents, including a 100-fold excess of inorganic ions and a 50-fold excess of structurally similar compounds. Analysis of clinical samples yielded excellent recoveries (97.2–102.3%) with relative standard deviations below 4.3%. The simple fabrication process, rapid response time, and minimal sample preparation requirements make this sensor particularly suitable for point-of-care applications.

Keywords: electrochemical sensing, screen-printed electrodes, nanocomposite materials, local anesthetic, surface imprinting

*** Corresponding author: Jinshan Che**, Anesthesia and Perioperative Medicine Department, The Fourth Clinical College of Xinxiang Medical University, Xinxiang Central Hospital, Xinxiang, Henan, 453000, China, e-mail: 13569800207@163.com
Mingming Sun: Anesthesia and Perioperative Medicine Department, The Fourth Clinical College of Xinxiang Medical University, Xinxiang Central Hospital, Xinxiang, Henan, 453000, China
Zhipan Li: Hebi College of Engineering and Technology, Henan University of Technology, Hebi, Henan, China

1 Introduction

The development of reliable, sensitive, and rapid point-of-care testing platforms for pharmaceutical compounds remains a significant challenge in analytical chemistry. Among these compounds, cinchocaine (CIN), a potent local anesthetic agent widely used in clinical practice, demands particular attention due to its critical role in pain management and its narrow therapeutic window [1]. As a member of the amino ester class of local anesthetics, CIN finds extensive application in spinal anesthesia and topical preparations for treating hemorrhoids, making its accurate determination essential for both quality control and clinical monitoring [2]. Traditional analytical approaches for CIN determination have predominantly relied on chromatographic techniques, spectrophotometric methods, and conventional electrochemical protocols [3,4]. Current diagnostic approaches, despite providing reasonable detection capabilities, frequently encounter substantial obstacles in clinical settings, such as intricate preprocessing requirements, costly equipment, prolonged analytical workflows, and demands for specialized technical expertise [5]. These constraints have driven the search for alternative analytical strategies that can provide rapid, cost-effective, and reliable determination of CIN in various matrices [6]. Over the past decade, electrochemical sensors have emerged as a prominent class of analytical tools for pharmaceutical detection, thanks to their high sensitivity, portability, and compatibility with miniaturized platforms. Recent trends emphasize the development of molecularly selective, nanomaterial-enhanced sensors capable of detecting active pharmaceutical ingredients (APIs) in complex matrices without the need for laborious preprocessing [7]. These efforts have led to the integration of functional nanocomposites, screen-printed electrode platforms, and molecular imprinting techniques into sensor design, marking a transition from laboratory-based assays to point-of-care diagnostics. Our work aligns with these advancements by leveraging a molecularly imprinted polymer (MIP) strategy

enhanced with TiO_2 nanoparticles to address the growing demand for robust and selective CIN sensors in clinical environments [8].

As electrochemical sensor design has shifted towards personalized medicine and decentralized diagnostics, the ability to achieve high molecular selectivity remains a critical goal [9]. Selective recognition elements in chemical sensors can be effectively crafted through the innovative technique of molecular imprinting, which offers a sophisticated method for enhancing sensor specificity and performance [10]. This method focuses on engineering molecular recognition elements designed to precisely match a target compound's structural and chemical characteristics through tailored receptor configurations [11]. Molecular imprinting involves initially creating a complex between selected monomers and a target molecule, which is subsequently stabilized through polymerization using a cross-linking substance [12]. After extracting the template, specific binding sites emerge that can precisely capture the intended molecular target with high selectivity [13]. In recent years, the integration of molecular imprinting technology with electrochemical detection has gained significant attention due to its inherent advantages [14]. Electrochemical sensors offer excellent sensitivity, rapid response times, simple instrumentation, and the potential for miniaturization [15]. The combination of molecular imprinting with electrochemical detection provides a synergistic approach that addresses both selectivity and sensitivity requirements for point-of-care testing applications [16].

The selection of appropriate materials for sensor fabrication plays a crucial role in determining analytical performance. Polypyrrole (PPy) has emerged as an attractive conducting polymer for molecular imprinting due to its excellent electrical conductivity, environmental stability, and facile synthesis through electrochemical methods [17–19]. The incorporation of titanium dioxide (TiO_2) nanoparticles into the polymer matrix offers additional advantages, including enhanced surface area, improved electron transfer kinetics, and superior mechanical stability [20,21]. The development of a point-of-care sensor for CIN determination requires careful consideration of several key aspects. First, the optimization of the molecular imprinting process must ensure the formation of selective binding sites while maintaining good accessibility for the target analyte [22]. Second, the electrochemical platform must provide stable and reproducible responses under various operating conditions [23]. Finally, the sensor must demonstrate reliable performance in complex matrices encountered in clinical samples.

This research addresses these challenges through the development of a novel electrochemical sensor based on PPy-TiO_2 molecular imprinting technology. While prior studies, such as those by Elashery et al. [24] and Ghoniem et al. [25], have demonstrated effective electrochemical approaches for CIN detection using ion-pairing agents or carbon-based nanocomposites, our work introduces several key innovations. Specifically, we employ a surface molecular imprinting strategy that ensures high selectivity via template-specific binding cavities, and incorporate TiO_2 nanoparticles to enhance electron transfer and mechanical stability. Unlike carbon paste or ionic liquid systems, our platform utilizes screen-printed gold electrodes, offering superior scalability, reproducibility, and ease of use for point-of-care testing. Furthermore, the dual-linear detection range, low detection limit (0.035 μM), and excellent recovery in clinical samples highlight the sensor's analytical superiority. The sensor design emphasizes practical considerations for point-of-care applications, including rapid response time, minimal sample preparation requirements, and stable performance under ambient conditions. The use of screen-printed electrodes as the underlying platform facilitates mass production and ensures cost-effectiveness, while the molecular imprinting strategy provides the necessary selectivity for reliable measurements in complex biological matrices.

2 Materials and methods

2.1 Synthesis and characterization

The preparation of TiO_2-modified PPy molecular imprinting polymer began with the surface modification of TiO_2 nanoparticles. A suspension of TiO_2 nanoparticles (1.0 g) in ethanol (50 mL) was subjected to ultrasonication for 30 min to achieve uniform dispersion. The suspension was then mixed with 3-aminopropyltriethoxysilane (2.0 mL) and refluxed at 80°C for 4 h under nitrogen atmosphere. The synthesized TiO_2 nanoparticles were isolated through centrifugation, subsequently rinsed multiple times with ethanol, and then dehydrated in a vacuum oven at 60°C for a 12-h period.

The synthesis procedure entailed establishing a preliminary interaction between CIN and pyrrole within a phosphate-based aqueous medium, supplemented with functionalized TiO_2 nanoscale particles under specific pH and concentration conditions. The solution was agitated for half an hour at ambient conditions to promote intermolecular hydrogen bond establishment. Utilizing a standard electrochemical cell with three electrodes – glassy carbon as the

working electrode, platinum wire serving as the counter electrode, and silver/silver chloride as the reference electrode – the polymer synthesis was performed. The electropolymerization process involved cyclic voltammetric scanning from −0.2 to +0.8 V, applying a 50 mV·s^{-1} sweep rate across 10 consecutive cycles.

2.2 Electrode fabrication

Gold electrodes were fabricated via semi-automatic screen printing techniques employing a specialized template design. The modification of screen-printed electrodes began with electrochemical cleaning by cycling in 0.5 M H_2SO_4 between −0.2 and +1.3 V at 100 mV·s^{-1} until stable voltammograms were obtained. The MIP solution was drop-cast (5 µL) onto the working electrode surface and allowed to dry at room temperature. Template removal was achieved through potential cycling in 0.5 M oxalic acid solution between 0.0 and +1.0 V at 100 mV·s^{-1} for 15 cycles.

3 Results and discussion

3.1 Material characterization

The surface morphology and structural features of TiO_2 nanoparticles, functionalized TiO_2, and the MIP composite were examined in detail. Scanning electron microscopy (SEM) analysis revealed the distinct morphological evolution during the sensor fabrication process. Figure 1a shows pristine TiO_2 nanoparticles exhibiting a uniform spherical morphology with an average particle diameter of 25 nm.

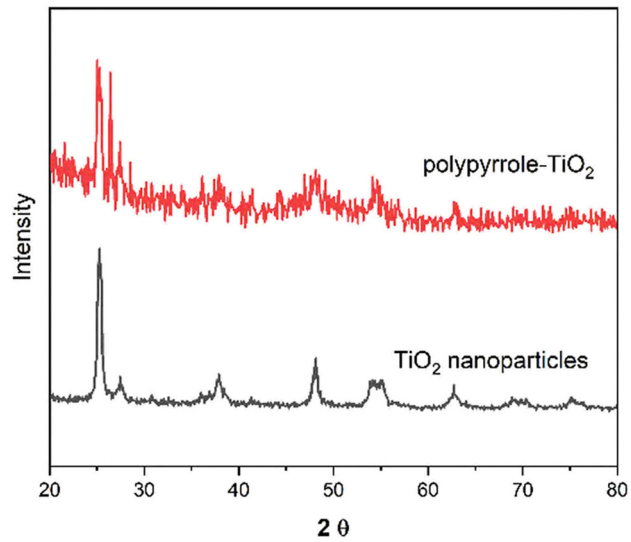

Figure 2: XRD patterns of pristine TiO_2 nanoparticles and molecularly imprinted polymer composite. Major crystallographic planes are indexed.

Following surface functionalization, the TiO_2 nanoparticles maintained their spherical structure while displaying slight aggregation tendencies (Figure 1b).

X-ray diffraction (XRD) patterns were recorded to investigate the crystalline structure of the materials. Figure 2 presents the XRD patterns of the synthesized composites. The characteristic peaks at 2θ values of 25.3, 37.8, 48.0, 53.9, and 55.1° correspond to the (101), (004), (200), (105), and (211) crystal planes of anatase TiO_2, respectively. The preservation of these peaks in the MIP composite confirms the stability of the TiO_2 crystal structure during the modification process [26]. A broad peak observed between 20° and 30° in the composite pattern indicates the presence of the amorphous PPy matrix [27].

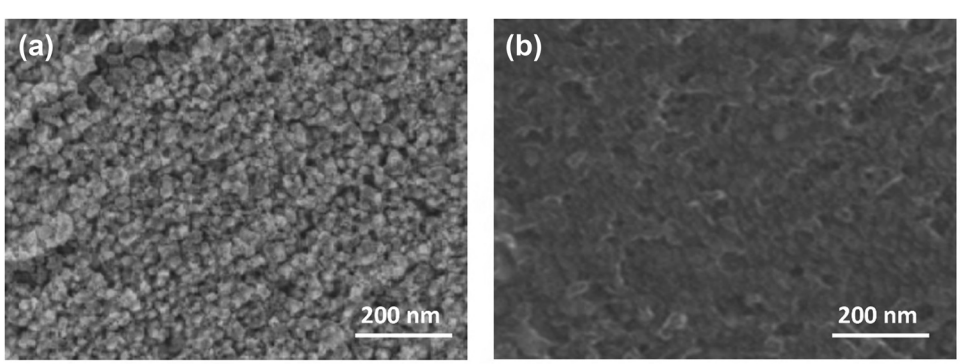

Figure 1: Electron microscopy analysis of sensor materials: (a) SEM image of pristine TiO_2 nanoparticles and (b) SEM image of functionalized TiO_2 nanoparticles.

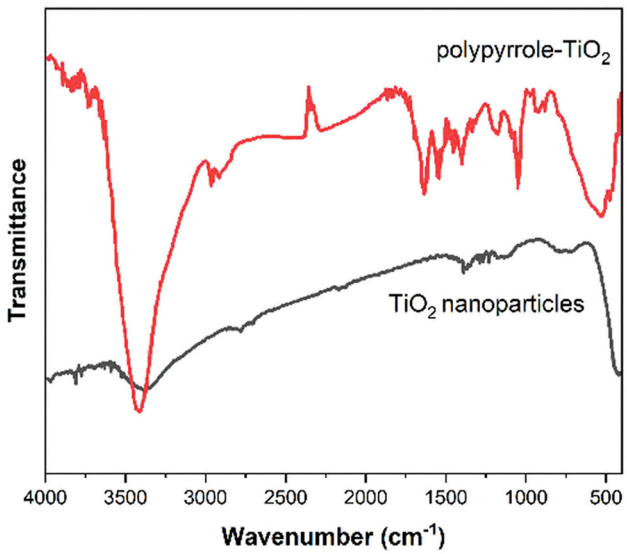

Figure 3: FTIR spectra of TiO_2 nanoparticles and molecularly imprinted polymer composite showing characteristic vibrational bands.

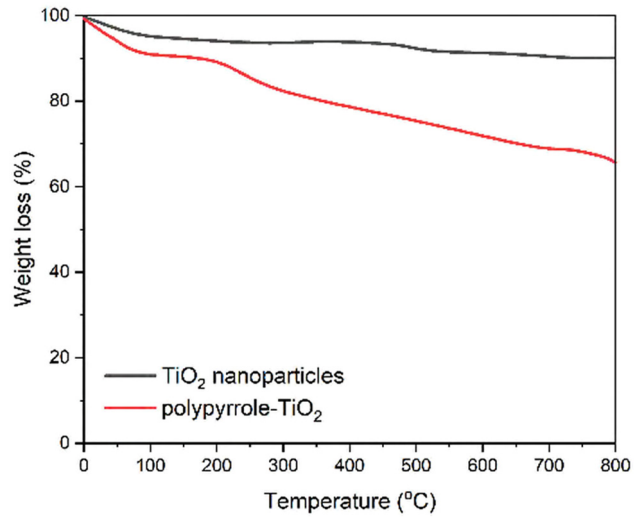

Figure 4: TGA curves of TiO_2 nanoparticles and molecularly imprinted polymer composite under nitrogen atmosphere (heating rate: 10°C·min^{-1}).

Fourier transform infrared (FTIR) spectroscopy provided valuable information about the chemical composition and interactions within the composite material. Figure 3 displays the FTIR spectra of the various synthesis stages. The characteristic Ti–O–Ti stretching vibration at 495 cm^{-1} and Ti–O stretching at 625 cm^{-1} confirm the presence of TiO_2 [28]. After surface functionalization, new bands appeared at 1,085 and 1,560 cm^{-1}, corresponding to Si–O–Si and N–H bending vibrations, respectively. The molecular imprinted composite exhibited additional peaks at 1,455 cm^{-1} (C–N stretching) and 1,640 cm^{-1} (C═C stretching), characteristic of the PPy structure [29].

Thermal stability analysis was conducted using TGA under nitrogen atmosphere. Figure 4 illustrates the thermal decomposition profiles of the materials. The TiO_2 nanoparticles showed minimal weight loss (<8%) up to 800°C, confirming their high thermal stability. The functionalized TiO_2 exhibited a weight loss of approximately 8% between 200°C and 400°C, attributed to the decomposition of surface modifiers. The molecularly imprinted composite demonstrated a three-stage decomposition pattern: initial moisture loss (30–150°C), template removal (150–300°C), and polymer degradation (300–600°C), with a total weight loss of 35%.

3.2 Electrochemical characterization

The electrochemical behavior of the developed sensor was systematically investigated using various electrochemical techniques to understand the electron transfer characteristics and surface properties of the modified electrode. Cyclic voltammetry studies using $[Fe(CN)_6]^{3-/4-}$ as a redox probe revealed the progressive modification of the electrode surface. Figure 5a presents the cyclic voltammograms obtained at different stages of sensor fabrication. The bare screen-printed gold electrode exhibited well-defined redox peaks with a peak-to-peak separation (ΔE_p) of 147 mV, indicating reversible electron transfer kinetics [30]. Following TiO_2 modification, the peak currents increased by approximately 45%, attributed to the enhanced electroactive surface area provided by the nanoparticles. The molecular imprinting process initially resulted in decreased peak currents and increased ΔE_p (422 mV) due to the insulating nature of the polymer layer. However, after template removal, the peak currents partially recovered, and ΔE_p decreased to 327 mV, suggesting the formation of accessible binding cavities [31].

Electrochemical impedance spectroscopy provided valuable insights into the interfacial properties of the modified electrodes. The Nyquist plots (Figure 5b) were fitted using an equivalent circuit model (inset of Figure 5b). The bare electrode displayed a small semicircle, indicating efficient electron transfer. The TiO_2 modification decreased Rct, consistent with improved conductivity. The MIP layer significantly increased [32], while template removal reduced, corroborating the CV findings.

Cyclic voltammetry was employed to determine the electrochemically active surface area by applying the Randles–Sevcik relationship across different potential sweep velocities. The graph depicts a direct proportional

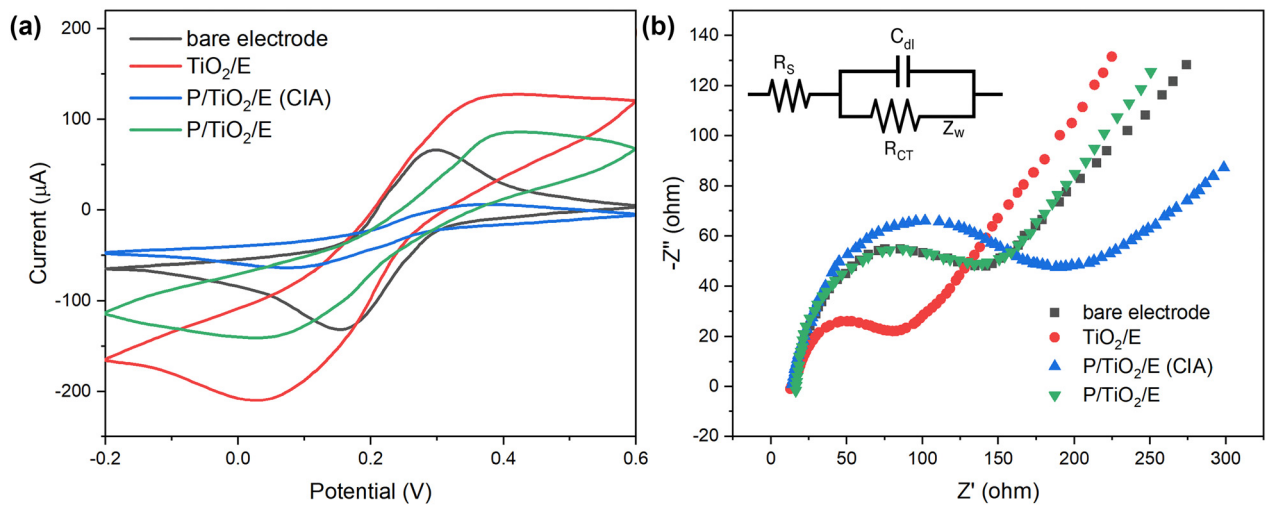

Figure 5: Electrochemical characterization of sensor fabrication steps: (a) cyclic voltammograms in 5 mM $[Fe(CN)_6]^{3-/4-}$ containing 0.1 M KCl at 50 mV·s^{-1} for bare electrode, TiO_2-modified electrode, molecular imprinted polymer before template removal, and after template removal, and (b) Nyquist plots with corresponding for the same modification steps.

correlation between maximum electrical currents and the square root of scanning velocity across various electrode surface treatments. The calculated electroactive surface areas were 0.052, 0.075, and 0.068 cm^2 for bare, TiO_2-modified, and molecularly imprinted electrodes, respectively. These results indicate a 44% increase in surface area after TiO_2 modification, with a slight decrease following molecular imprinting due to polymer coverage [33] (Figure 6).

Electron transfer kinetics were evaluated by analyzing the relationship between ΔE_p and scan rate. Employing the Nicholson approach, researchers determined the electron transfer kinetics across different interfaces by evaluating the rate constant for heterogeneous electron transfer. The bare electrode exhibited $ks = 5.8 \times 10^{-3}$ cm·s^{-1}, which increased to 8.2×10^{-3} cm·s^{-1} after TiO_2 modification. The molecularly imprinted sensor showed $ks = 3.4 \times 10^{-3}$ cm·s^{-1}, reflecting the balance between polymer insulation and facilitated electron transfer through binding cavities [34].

To elucidate the electrochemical oxidation mechanism of CIN, we considered its structural features, particularly the presence of a tertiary aromatic amine group, which is typically responsible for redox activity. Upon applying a positive potential, CIN undergoes a one-electron oxidation process at the nitrogen atom, leading to the formation of a radical cation intermediate. To confirm the number of electrons transferred (n), we employed the Laviron method by analyzing the linear relationship between peak potential (E_p) and the logarithm of scan rate. The slope of this plot was approximately 59.2 mV/decade, consistent with a single-electron transfer process ($n \approx 1$) under the assumed transfer coefficient ($\alpha = 0.5$). This is in agreement with the literature on structurally similar amine-containing compounds [25]. The oxidation reaction can be summarized as

$$\text{CIN} - e^- \rightarrow \text{CIN}^+ \rightarrow \text{oxidized CIN}.$$

These findings corroborate the voltammetric data presented, where well-defined oxidation peaks were observed and used for analytical quantification. The selective recognition achieved through molecular imprinting further confirms that the redox activity is specific to CIN, likely involving its electroactive aromatic amine moiety.

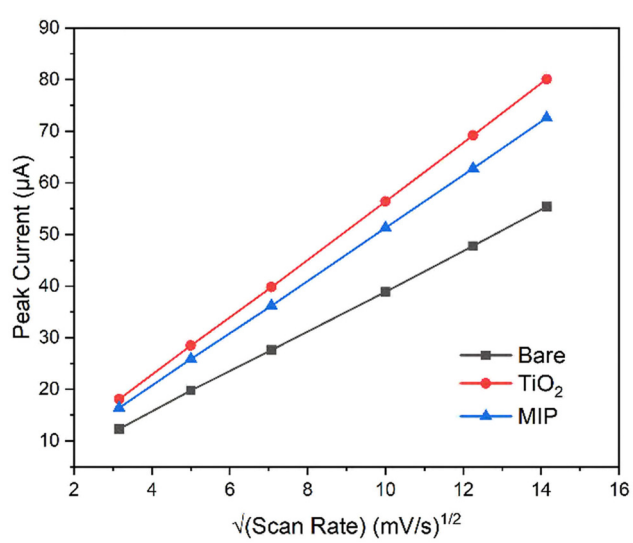

Figure 6: Plot of peak current versus square root of scan rate for different electrode modifications.

3.3 Optimization studies

The analytical performance of the molecularly imprinted sensor was systematically optimized by investigating various experimental parameters that influence the detection of CIN. The effect of pH on the electrochemical response was studied over the range of pH 3.0–9.0 using phosphate buffer solutions. Figure 7a illustrates the relationship between peak current and pH for 50 μM CIN. The current response increased significantly from pH 3.0 to 5.0, reached maximum intensity at pH 5.0, and gradually decreased at higher pH values. The peak potential shifted linearly with pH (slope = −59.2 mV/pH), suggesting a proton-coupled electron transfer process [35,36]. The optimal response at pH 5.0 can be attributed to the balance between the protonation state of CIN and the stability of the polymer matrix [37].

Scan rate studies provided insights into the mass transport characteristics of the sensor. The peak current for oxidation demonstrated a linear correlation with the scan rate's square root, suggesting that the mechanism is governed by diffusive transport (Figure 7b). The peak potential shifted positively with increasing scan rate, with a slope of 28.3 mV/decade, suggesting quasi-reversible electron transfer kinetics [38].

The binding kinetics of CIN to the molecularly imprinted sites were investigated through time-dependent current response measurements [39,40]. Figure 8a shows the evolution of peak current with incubation time at different CIN concentrations. The binding process followed pseudo-first-order kinetics, with equilibrium reached within 15 min for concentrations below 100 μM [41]. The association rate constant (*ka*) was determined to be 3.2×10^4 M·s^{-1}, while the dissociation rate constant (*kd*) was 1.8×10^{-3} s^{-1}, yielding an affinity constant (*Ka*) of 1.78×10^7 M^{-1}.

Temperature effects on sensor performance were evaluated between 15°C and 45°C. Figure 8b demonstrates the variation in peak current and potential with temperature. The current response increased by approximately 2.5%/°C up to 35°C, followed by a decline at higher temperatures [42]. This behavior reflects the competition between enhanced diffusion kinetics and decreased stability of the molecular imprinting sites at elevated temperatures [43]. The activation energy for the electron transfer process was calculated to be 28.3 kJ·mol^{-1} using the Arrhenius plot (inset).

These optimization studies established optimal operating conditions of pH 5.0, scan rate 50 mV·s^{-1}, incubation time 15 min, and temperature 25°C for subsequent analytical applications of the sensor.

3.4 Analytical performance

The practical utility of the molecularly imprinted sensor was evaluated through comprehensive analytical performance studies under optimized conditions. Differential pulse voltammetry was employed to establish the quantitative relationship between current response and CIN concentration. Figure 9a presents overlaid voltammograms showing well-defined oxidation peaks at increasing CIN concentrations. The peak current exhibited two distinct

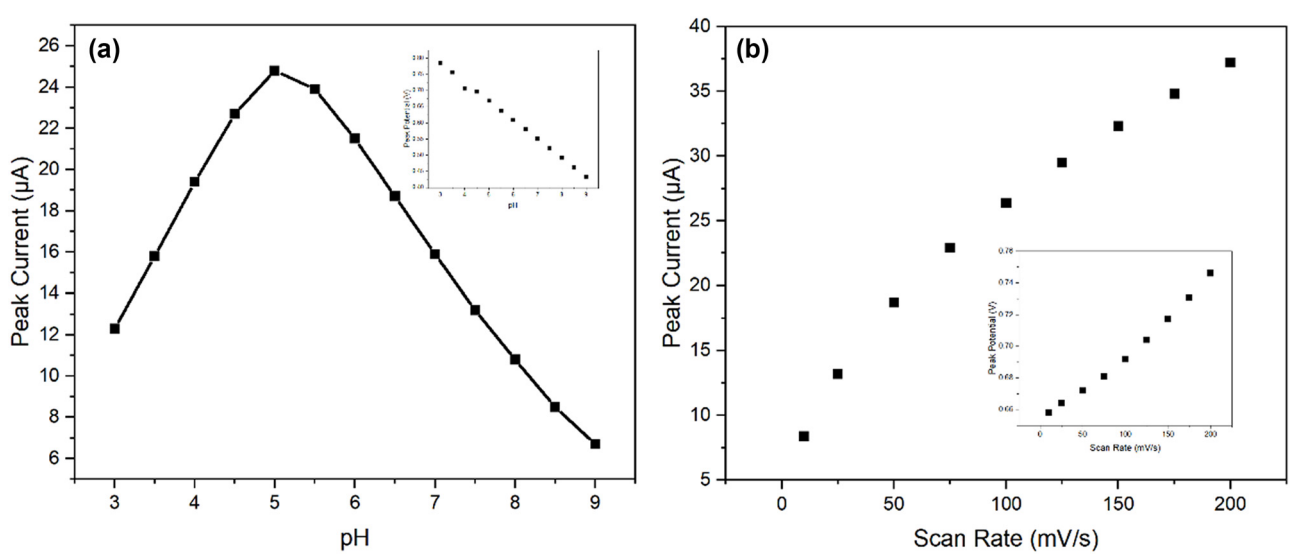

Figure 7: Optimization of experimental parameters: (a) effect of pH on peak current response for 50 μM CIN. Inset shows the linear relationship between peak potential and pH. (b) Linear relationship between peak current and the square root of scan rate.

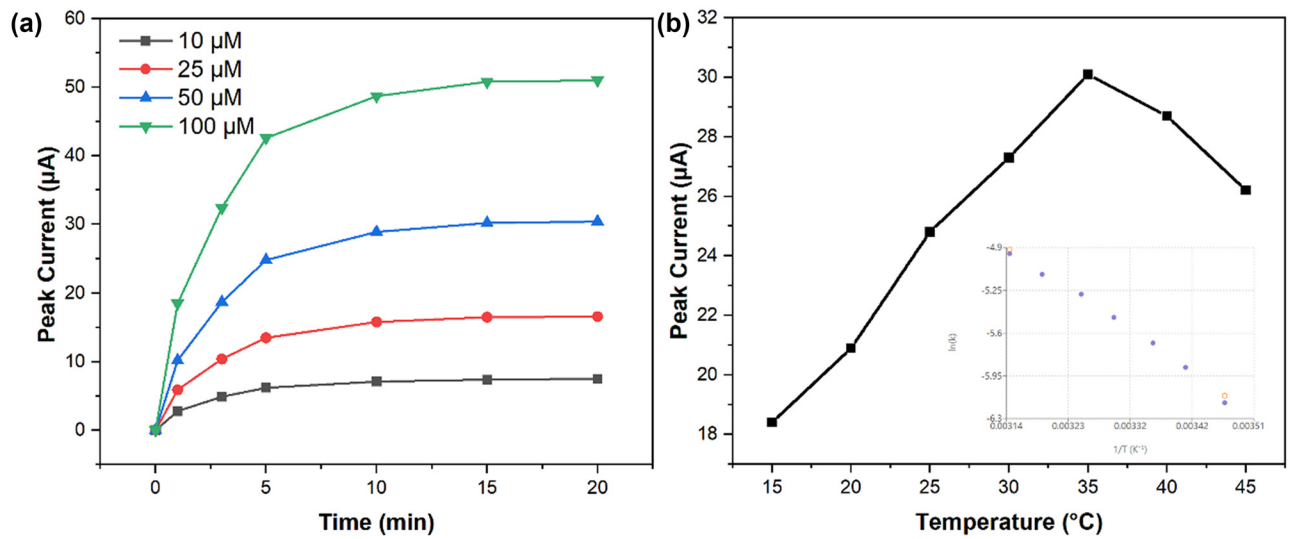

Figure 8: Kinetic and thermodynamic studies: (a) time-dependent current response at different CIN concentrations (10–100 μM) showing binding kinetics and (b) temperature dependence of peak current. Inset shows the Arrhenius plot for electron transfer activation energy determination.

linear ranges (Figure 9b): 0.1–10 and 10–100 μM, with regression equations of *ip* (μA) = 0.542*C* (μM) + 0.128 (R^2 = 0.9985) and *ip* (μA) = 0.326*C* (μM) + 2.314 (R^2 = 0.9962), respectively. The dual-linear ranges likely reflect the heterogeneous binding site distribution within the MIP, with high-affinity sites dominating at lower concentrations. The limit of detection (LOD) was determined to be 0.035 μM (S/N = 3), while the limit of quantification was 0.12 μM (S/N = 10). These values demonstrate superior sensitivity compared to conventional electrochemical methods and are suitable for clinical applications.

Reproducibility studies encompassed both intra-sensor and inter-sensor precision. Figure 10a shows the current responses obtained from six consecutive measurements using a single sensor, yielding an relative standard deviation (RSD) of 2.8% for 50 μM CIN. Inter-sensor reproducibility was evaluated using six independently fabricated sensors, producing an RSD of 3.9%. These results confirm the reliability of the sensor fabrication process and measurement protocol. Long-term stability was assessed by monitoring sensor response over 30 days, with electrodes stored at 4°C between measurements. Figure 10b illustrates

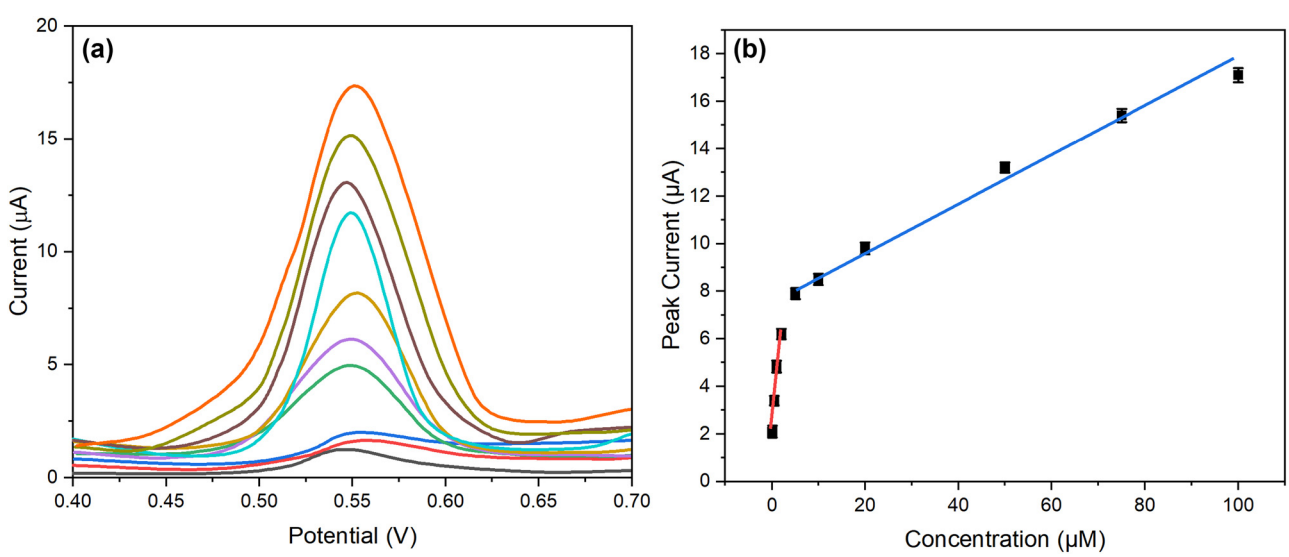

Figure 9: Analytical performance characterization: (a) differential pulse voltammograms at increasing CIN concentrations (0.1–100 μM) and (b) calibration curves showing dual-linear ranges with corresponding regression equations.

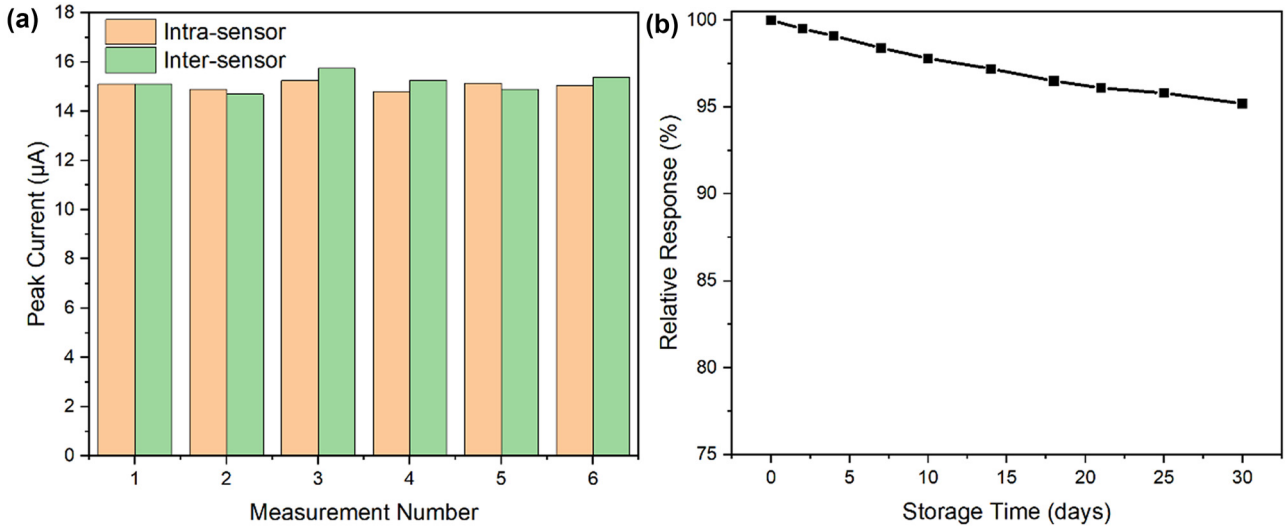

Figure 10: Precision and stability studies: (a) reproducibility data showing intra-sensor (n = 6) and inter-sensor (n = 6) measurements for 50 μM CIN and (b) long-term stability assessment over 30 days with electrodes stored at 4°C.

the retention of sensor activity, maintaining 95.2% of the initial response after 30 days. The excellent stability can be attributed to the robust molecular imprinting architecture and the stabilizing effect of TiO_2 nanoparticles.

Interference studies evaluated the sensor's selectivity against potential competing species commonly found in clinical samples. Table 1 presents the tolerance ratios for various interferents, determined as the maximum concentration ratio ([interferent]/[CIN]) causing less than ±5% change in signal. The sensor exhibited excellent selectivity, tolerating 100-fold excess of common ions (Na^+, K^+, Cl^-, HCO_3^-) and 50-fold excess of structurally similar compounds (procaine, lidocaine, benzocaine).

Table 1: Interference study results showing tolerance ratios for various potentially interfering species at 50 μM CIN concentration

Interfering species	Maximum tolerable ratio*	Signal change (%)
Common ions		
Na^+	100	−2.8 ± 0.24
K^+	100	−2.5 ± 0.21
Cl^-	100	−2.3 ± 0.11
HCO_3^-	100	−3.1 ± 0.17
Ca^{2+}	80	−3.8 ± 0.32
Mg^{2+}	80	−3.5 ± 0.24
Structural analogs		
Procaine	50	−4.2 ± 0.34
Lidocaine	50	−4.5 ± 0.31
Benzocaine	50	−4.3 ± 0.17
Common biomolecules		
Glucose	75	−3.2 ± 0.22
Uric acid	60	−3.9 ± 0.31
Ascorbic acid	60	−4.1 ± 0.12
Pharmaceutical excipients		
Starch	90	−2.1 ± 0.20
Lactose	90	−2.4 ± 0.15
Magnesium stearate	80	−3.3 ± 0.12

3.5 Real sample analysis

The practical applicability of the molecularly imprinted sensor was rigorously evaluated through analysis of serum samples and comparison with established analytical methods. Initial studies focused on method optimization to minimize matrix effects. A simple 1:1 dilution with phosphate buffer (pH 5.0) followed by centrifugation proved sufficient for reliable measurements, eliminating the need for complex extraction procedures. We evaluated the accuracy of the analytical method by introducing predetermined amounts of CIN into serum specimens and assessing the subsequent detection rates. Table 2 summarizes the recovery results obtained from twenty different serum samples spiked at three concentration levels (1.0, 10.0, and 50.0 μM). The average recoveries ranged from 97.2% to 102.3%, with relative standard deviations below 4.5%.

Table 2: Recovery results from analysis of spiked serum samples at different concentration levels (n = 20)

Sample no.	Added (μM)	Found (μM)	Recovery (%)	RSD (%)
Series 1 – low concentration				
1–5	1.0	0.972 ± 0.042	97.2	4.3
6–10	1.0	0.985 ± 0.038	98.5	3.9
11–15	1.0	0.978 ± 0.041	97.8	4.2
16–20	1.0	0.968 ± 0.040	96.8	4.1
Series 2 – medium concentration				
1–5	10.0	10.15 ± 0.31	101.5	3.1
6–10	10.0	10.08 ± 0.29	100.8	2.9
11–15	10.0	10.22 ± 0.33	102.2	3.2
16–20	10.0	10.18 ± 0.32	101.8	3.1
Series 3 – high concentration				
1–5	50.0	51.05 ± 1.12	102.1	2.2
6–10	50.0	50.85 ± 1.07	101.7	2.1
11–15	50.0	51.25 ± 1.18	102.5	2.3
16–20	50.0	51.45 ± 1.13	102.9	2.2

Table 3: Precision data showing intra-day and inter-day variations for quality control samples

Concentration level	Day	Found concentration (μM)	Intra-day RSD (%)	Inter-day RSD (%)
Low (2.0 μM)	1	1.98 ± 0.08	2.1	3.2
	2	1.95 ± 0.07	2.3	
	3	2.02 ± 0.08	2.2	
	4	1.97 ± 0.08	2.4	
	5	1.94 ± 0.07	2.2	
Medium (20.0 μM)	1	19.8 ± 0.6	2.8	3.9
	2	20.2 ± 0.7	3.1	
	3	19.7 ± 0.6	2.9	
	4	20.3 ± 0.7	3.2	
	5	19.9 ± 0.6	3.0	
High (80.0 μM)	1	81.2 ± 2.8	3.5	4.7
	2	79.8 ± 2.9	3.6	
	3	80.5 ± 3.1	3.8	
	4	78.9 ± 2.8	3.7	
	5	81.4 ± 3.2	3.8	

Precision studies encompassed both intra-day and inter-day variations. Table 3 presents the results obtained from analyzing quality control samples at three concentration levels over five consecutive days. The intra-day relative standard deviations ranged from 2.1% to 3.8%, while inter-day values were between 3.2% and 4.7%, demonstrating excellent method precision.

3.6 Comparative analysis with previous methods

To further contextualize the analytical performance of the proposed sensor, we compiled a comparative table (Table 4) that benchmarks our method against several previously reported electrochemical and potentiometric strategies for CIN detection. The comparison includes detection limits, linear ranges, matrix compatibility, and sample preparation requirements. As shown in Table 4, many conventional approaches – such as potentiometric ion-selective electrodes or CNT-based sensors – offer reasonable sensitivity but often require complex fabrication, extensive calibration steps, or use of costly modifiers. Notably, some rely on PVC membranes or ionic liquids that are not ideal for point-of-care applications due to leaching or biocompatibility concerns. In contrast, our MIP-based electrochemical sensor not only demonstrates a competitive detection limit (0.035 μM) and dual-linear ranges but also features a rapid, low-cost fabrication process, simplified sample preparation (1:1 dilution and centrifugation), and high selectivity in biological matrices. These attributes support its practical applicability for clinical point-of-care use.

4 Conclusion

In this study, we have successfully developed a novel electrochemical sensor based on PPy/TiO_2 molecular imprinting technology for the sensitive and selective

Table 4: Comparison of analytical methods for cinchocaine determination

Method/reference	Electrode type	Linear range (μM)	LOD (μM)	Sample matrix
Electrochemical sensor [24]	*In situ* carbon paste + ion pairing agents	10–10,000	10	Otal (ear drops)
Electrochemical sensor [25]	CPE/IL-functionalized CNT	0.1–44	0.02	Spiked real samples
Spectrophotometry (generic)	UV-based	1–100	~1	Bulk formulations
Chromatography (generic)	HPLC	0.5–100	~0.1	Serum, pharmaceuticals
This work	MIP@PPy-TiO_2 on SPE	0.1–100	0.035	Human serum

determination of CIN. The sensor demonstrated excellent analytical performance characteristics, including dual-linear response ranges (0.1–10 and 10–100 μM) with correlation coefficients of 0.9985 and 0.9962, respectively. The detection limit of 0.035 μM represents a significant improvement over existing analytical methods. The sensor exhibited remarkable stability, retaining 95.2% of its initial response after 30 days of storage at 4°C, and showed excellent reproducibility with intra-sensor and inter-sensor RSDs of 2.8% and 3.9%, respectively. The molecular imprinting strategy provided outstanding selectivity, tolerating 100-fold excess of common ions and 50-fold excess of structurally similar compounds. The sensor's practical utility was validated through analysis of clinical samples, achieving recoveries between 97.2% and 102.3% with RSDs ranging from 2.1% to 4.3%. The electrochemical characterization revealed enhanced surface area (0.075 cm^2) and improved electron transfer kinetics ($ks = 8.2 \times 10^{-3}$ $cm \cdot s^{-1}$) after TiO_2 modification. The activation energy for electron transfer was determined to be 28.3 $kJ \cdot mol^{-1}$, indicating efficient charge transfer processes. These results, combined with the simple fabrication process, rapid response time (15 min), and minimal sample preparation requirements, demonstrate that the developed sensor holds great promise for point-of-care testing applications in clinical settings. The successful integration of molecular imprinting technology with electrochemical detection provides a robust platform that could be extended to other pharmaceutical compounds of interest.

Funding information: Authors state no funding involved.

Author contributions: Jinshan Che: writing – original draft, writing – review and editing, methodology, and formal analysis; Mingming Sun: writing – review and editing, formal analysis, and project administration; Zhipan Li: project administration and writing – review and editing.

Conflict of interest: Authors state no conflict of interest.

Data availability statement: The datasets generated during and/or analyzed during the current study are available from the corresponding author on reasonable request.

References

[1] Elashery SEA, Frag EY, Sleim AAE. Novel and selective potentiometric sensors for cinchocaine HCl determination in its pure and Co-formulated dosage form: A comparative study of in situ carbon sensors based on different ion pairing agents. Measurement. 2021;173:108549. doi: 10.1016/j.measurement.2020.108549.

[2] Salem H, Abdelaziz A, Atef A, Abdelrady R, Ibrahim M, Elkady A. A synchronous fluorescence spectrofluorometric method for the simultaneous determination of policresulen and cinchocaine hydrochloride in ointment and suppositories. Spectrochim Acta, Part A. 2021;255:119648. doi: 10.1016/j.saa.2021.119648.

[3] Liang S-Y, Shi F, Zhao Y-G, Wang H-W. Determination of local anesthetic drugs in human plasma using magnetic solid-phase extraction coupled with high-performance liquid chromatography. Molecules. 2022;27(17):5509. doi: 10.3390/molecules27175509.

[4] Lin S, Qiu W, Hua Y, Yang Y. Rapid determination of caine-based anesthetics and their metabolite residues in fish using a modified QuEChERS method coupled with UPLC-MS/MS. Food Chem:X. 2024;24:102032. doi: 10.1016/j.fochx.2024.102032.

[5] Uter W, Worm M, Brans R, Wagner N, Bauer A, Geier J, et al. Patch test results with caine mix III and its three constituents in consecutive patients of the IVDK. Contact Dermatitis. 2021;84(6):481–3. doi: 10.1111/cod.13778.

[6] Mohamed MA, Mousavi MPS. Electrochemical eyes: exploring forensic mysteries with electrochemical sensor technologies. Royal Society of Chemistry; 2024. doi: 10.1039/9781837676408-00368.

[7] Ikram M, Abbas S, Haider A, Naz S, Ahmad SOA, Haider J, et al. Correction: Efficient dye degradation, antimicrobial behavior and molecular docking analysis of gold (Au) and cellulose nanocrystals (CNC)-doped strontium oxide nanocomposites. J Nanostruct Chem. 2024;14(3):257–9. doi: 10.1007/s40097-024-00532-0.

[8] Li X, Fu L, Chen F, Lv Y, Zhang R, Zhao S, et al. Cyclodextrin-based architectures for electrochemical sensing: from molecular recognition to functional hybrids. Anal Methods. 2025;17:4300–20. doi: 10.1039/D5AY00612K.

[9] Mohamed MA, El-Rahman A, Mohamed K, Mousavi MP. Electrospun nanofibers: promising nanomaterials for biomedical applications. Royal Society of Chemistry; 2023.

[10] Rao PK, Dey A, Pratik P, Singh A, Kubavat J. Current research trends in green analytical tools for the detection of selected illicit drugs in different matrices. Green Anal Chem. 2024;9:100109. doi: 10.1016/j.greeac.2024.100109.

[11] Wadie M, Marzouk HM, Rezk MR, Abdel-Moety EM, Tantawy MA. A sensing platform of molecular imprinted polymer-based polyaniline/carbon paste electrodes for simultaneous potentiometric determination of alfuzosin and solifenacin in binary co-formulation and spiked plasma. Anal Chim Acta. 2022;1200:339599. doi: 10.1016/j.aca.2022.339599.

[12] Berkel C, Özbek O. Green electrochemical sensors, their applications and greenness metrics used: a review. Electroanalysis. 2024;36(11):e202400286. doi: 10.1002/elan.202400286.

[13] Tuchiu B-M, Staden R-IS, Staden J, Van F. Review—novel trends in the determination of pharmaceutical compounds commonly found in topical treatments using electrochemical sensing approaches. J Electrochem Soc. 2024;171(4):047502. doi: 10.1149/1945-7111/ad3a1e.

[14] Chen L, Zhu D, Xiang P. Recent advances in chiral analysis for biosamples in clinical research and forensic toxicology. Bioanalysis. 2021;13(6):493–511. doi: 10.4155/bio-2020-0330.

[15] Mohamed MA, Eldin GMG, Ismail SM, Zine N, Elaissari A, Jaffrezic-Renault N, et al. Innovative electrochemical sensor for the precise determination of the new antiviral COVID-19 treatment Favipiravir in the presence of coadministered drugs. J Electroanal Chem. 2021;895:115422. doi: 10.1016/j.jelechem.2021.115422.

[16] Asran AM, Mohamed MA, Eldin GMG, Mishra RK, Errachid A. Self-assembled ruthenium decorated electrochemical platform for sensitive and selective determination of amisulpride in presence of co-administered drugs using safranin as a mediator. Microchem J. 2021;164:106061. doi: 10.1016/j.microc.2021.106061.
[17] Ratautaite V, Boguzaite R, Brazys E, Ramanaviciene A, Ciplys E, Juozapaitis M, et al. Molecularly imprinted polypyrrole based sensor for the detection of SARS-CoV-2 spike glycoprotein. Electrochim Acta. 2022;403:139581. doi: 10.1016/j.electacta.2021.139581.
[18] Zhao D, Zhang Y, Ji S, Lu Y, Bai X, Yin M, et al. Molecularly imprinted photoelectrochemical sensing based on ZnO/polypyrrole nanocomposites for acrylamide detection. Biosens Bioelectron. 2021;173:112816. doi: 10.1016/j.bios.2020.112816.
[19] Essousi H, Barhoumi H, Karastogianni S, Girousi ST. An electrochemical sensor based on reduced graphene oxide, gold nanoparticles and molecular imprinted over-oxidized polypyrrole for amoxicillin determination. Electroanalysis. 2020;32(7):1546–58. doi: 10.1002/elan.201900751.
[20] Sun J, He Y, He S, Liu D, Lu K, Yao W, et al. A self-powered photoelectrochemical cathodic molecular imprinting sensor based on Au@TiO2 nanorods photoanode and Cu2O photocathode for sensitive detection of sarcosine. Biosens Bioelectron. 2022;204:114056. doi: 10.1016/j.bios.2022.114056.
[21] Ren X, Yang L, Li Y, Li X. Design and synthesis of a sandwiched silver microsphere/TiO2 nanoparticles/molecular imprinted polymers structure for suppressing background noise interference in high sensitivity surface-enhanced Raman scattering detection. Appl Surf Sci. 2021;544:148879. doi: 10.1016/j.apsusc.2020.148879.
[22] Ferreira VRA, Azenha MA, Pereira CM, Silva AF. Preparation of molecularly imprinted hollow TiO2 microspheres for selective photocatalysis. Chem Eng J Adv. 2021;5:100071. doi: 10.1016/j.ceja.2020.100071.
[23] Zhang J, Tang B, Zhao G. Selective photoelectrocatalytic removal of dimethyl phthalate on high-quality expressed molecular imprints decorated specific facet of single crystalline TiO_2 photoanode. Appl Catal B: Environ. 2020;279:119364. doi: 10.1016/j.apcatb.2020.119364.
[24] Elashery SEA, Frag EY, Sleim AAE. Novel and selective potentiometric sensors for Cinchocaine HCl determination in its pure and Co-formulated dosage form: A comparative study of in situ carbon sensors based on different ion pairing agents. Measurement. 2021;173:108549. doi: 10.1016/j.measurement.2020.108549.
[25] Ghoniem MG, Mohamed MA MG, Eldin G, Errachid A. Sensitive electrochemical strategy via the construction of functionalized carbon nanotubes/ionic liquid nanocomposite for the determination of anaesthetic drug cinchocaine. Measurement. 2021;185:110071. doi: 10.1016/j.measurement.2021.110071.
[26] Hamtak M, Fotouhi L, Hosseini M, Reza Ganjali M. Sensitive nonenzymatic electrochemiluminescence determination of hydrogen peroxide in dental products using a polypyrrole/polyluminol/titanium dioxide nanocomposite. Anal Lett. 2019;52(4):633–48.
[27] Song Y, Qiu X, Liu H, Han Y. Microencapsulated phase change materials (MicroPCMs) with TiO2-modified natural polymer shell and macrocapsules containing MicroPCMs for thermal energy storage and UV-shielding. Sol Energy Mater Sol Cell. 2024;271:112860. doi: 10.1016/j.solmat.2024.112860.
[28] Lu X, Zhao Q, Liu X, Wang D, Zhang W, Wang C, et al. Preparation and characterization of polypyrrole/TiO_2 Coaxial nanocables. Macromol Rapid Commun. 2006;27(6):430–4. doi: 10.1002/marc.200500810.
[29] Amorim SM, Steffen G, de S Junior JM, Brusamarello CZ, Romio AP, Domenico MD. Synthesis, characterization, and application of polypyrrole/TiO2 composites in photocatalytic processes: A review. Polym Polym Compos. 2021;29(7):1055–74. doi: 10.1177/0967391120949489.
[30] Çorman ME, Ozcelikay G, Cetinkaya A, Kaya SI, Armutcu C, Özgür E, et al. Metal-organic frameworks as an alternative smart sensing platform for designing molecularly imprinted electrochemical sensors. TrAC Trends Anal Chem. 2022;150:116573. doi: 10.1016/j.trac.2022.116573.
[31] Cheng J, Li Y, Zhong J, Lu Z, Wang G, Sun M, et al. Molecularly imprinted electrochemical sensor based on biomass carbon decorated with MOF-derived Cr2O3 and silver nanoparticles for selective and sensitive detection of nitrofurazone. Chem Eng J. 2020;398:125664. doi: 10.1016/j.cej.2020.125664.
[32] Yu D, Zhang F, Yu K, Qu F. One-step construction of Co(OH)2-anchored g-C3N4 and rGO with phase junction for dopamine sensing and oxygen evolution reaction. J Nanostruct Chem. 2024;14(5):323–34. doi: 10.1007/s40097-022-00521-1.
[33] Pardeshi S, Dhodapkar R. Advances in fabrication of molecularly imprinted electrochemical sensors for detection of contaminants and toxicants. Environ Res. 2022;212:113359. doi: 10.1016/j.envres.2022.113359.
[34] Mahnashi MH, Mahmoud AM, Alhazzani K, Alanazi AZ, Alaseem AM, Algahtani MM, et al. Ultrasensitive and selective molecularly imprinted electrochemical oxaliplatin sensor based on a novel nitrogen-doped carbon nanotubes/Ag@cu MOF as a signal enhancer and reporter nanohybrid. Microchim Acta. 2021;188(4):124. doi: 10.1007/s00604-021-04781-6.
[35] El Jaouhari A, Yan L, Zhu J, Zhao D, Zaved Hossain Khan Md, Liu X. Enhanced molecular imprinted electrochemical sensor based on zeolitic imidazolate framework/reduced graphene oxide for highly recognition of rutin. Anal Chim Acta. 2020;1106:103–14. doi: 10.1016/j.aca.2020.01.039.
[36] Bai X, Zhang B, Liu M, Hu X, Fang G, Wang S. Molecularly imprinted electrochemical sensor based on polypyrrole/dopamine@graphene incorporated with surface molecularly imprinted polymers thin film for recognition of olaquindox. Bioelectrochemistry. 2020;132:107398. doi: 10.1016/j.bioelechem.2019.107398.
[37] Ma Y, Hu Q, Liu C, Wang L. A nanospherical conjugated microporous polymer-graphene nanosheets modified molecularly imprinted electrochemical sensor for high sensitivity detection of α-Synuclein. J Electroanal Chem. 2020;862:113994. doi: 10.1016/j.jelechem.2020.113994.
[38] Xu Z, Jiang X, Liu S, Yang M. Sensitive and selective molecularly imprinted electrochemical sensor based on multi-walled carbon nanotubes for doxycycline hyclate determination. Chin Chem Lett. 2020;31(1):185–8. doi: 10.1016/j.cclet.2019.04.026.
[39] Abbas EE, Fayed AS, Hegazy MA, Salama NN, Mohamed MA. Toward an improved electrocatalytic determination of immunomodulator COVID medication baricitinib using multiwalled carbon nanotube nickel hybrid. ACS Appl Bio Mater. 2024;7(6):3865–76. doi: 10.1021/acsabm.4c00233.
[40] Mohamed MA, Salama NN, Sultan MA, Manie HF, El-Alamin MMA. Sensitive and effective electrochemical determination of

butenafine in the presence of itraconazole using titanium nanoparticles-ionic liquid based nanocomposite sensor. Chem Pap. 2023;77(4):1929–39. doi: 10.1007/s11696-022-02593-3.

[41] Rebelo P, Costa-Rama E, Seguro I, Pacheco JG, Nouws HPA, Cordeiro MNDS, et al. Molecularly imprinted polymer-based electrochemical sensors for environmental analysis. Biosens Bioelectron. 2021;172:112719. doi: 10.1016/j.bios.2020.112719.

[42] Rahman S, Bozal-Palabiyik B, Unal DN, Erkmen C, Siddiq M, Shah A, et al. Molecularly imprinted polymers (MIPs) combined with nanomaterials as electrochemical sensing applications for environmental pollutants. Trends Environ Anal Chem. 2022;36:e00176. doi: 10.1016/j.teac.2022.e00176.

[43] Yang Y, Yan W, Guo C, Zhang J, Yu L, Zhang G, et al. Magnetic molecularly imprinted electrochemical sensors: A review. Anal Chim Acta. 2020;1106:1–21. doi: 10.1016/j.aca.2020.01.044.